Atmos. Chem. Phys. Discuss., 15, 10553–10592, 2015
www.atmos-chem-phys-discuss.net/15/10553/2015/
doi:10.5194/acpd-15-10553-2015

Atmospheric Chemistry and Physics Discussions

Secondary organic aerosol formation from photochemical aging of light-duty gasoline vehicle exhausts in a smog chamber

T. Liu[1,2], X. Wang[1,3], W. Deng[1,2], Q. Hu[1], X. Ding[1], Y. Zhang[1], Q. He[1,2], Z. Zhang[1,2], S. Lü[1,2], X. Bi[1], J. Chen[4], and J. Yu[5]

[1]State Key Laboratory of Organic Geochemistry, Guangzhou Institute of Geochemistry, Chinese Academy of Sciences, Guangzhou 510640, China
[2]University of Chinese Academy of Sciences, Beijing 100049, China
[3]Guangdong Key Laboratory of Environmental Protection and Resources Utilization, Guangzhou Institute of Geochemistry, Chinese Academy of Sciences, Guangzhou 510640, China
[4]Shanghai Key Laboratory of Atmospheric Particle Pollution and Prevention, Department of Environmental Science & Engineering, Fudan University, Shanghai 200433, China
[5]Division of Environment, Hong Kong University of Science & Technology, Clear Water Bay, Kowloon, Hong Kong, China

Received: 9 February 2015 – Accepted: 20 March 2015 – Published: 10 April 2015

Correspondence to: X. Wang (wangxm@gig.ac.cn)

Published by Copernicus Publications on behalf of the European Geosciences Union.

ACPD
15, 10553–10592, 2015

Abstract

In China, fast increase in passenger vehicles has procured the growing concern about vehicle exhausts as an important source of anthropogenic secondary organic aerosols (SOA) in megacities hard-hit by haze. However, there are still no chamber simulation studies in China on SOA formation from vehicle exhausts. In this study, the SOA formation of emissions from two idling light-duty gasoline vehicles (LDGVs) (Euro 1 and Euro 4) in China was investigated in a 30 m^3 smog chamber. Five photo-oxidation experiments were carried out at 25 °C with the relative humidity around 50 %. After aging at an OH exposure of 5×10^6 molecules cm^{-3} h, the formed SOA was 12–259 times as high as primary OA (POA). The SOA production factors (PF) were 0.001–0.044 g kg^{-1} fuel, comparable with those from the previous studies at the quite similar OH exposure. This quite lower OH exposure than that in typical atmospheric condition might however lead to the underestimation of the SOA formation potential from LDGVs. Effective SOA yield data in this study were well fit by a one-product gas-particle partitioning model and quite lower than those of a previous study investigating SOA formation form three idling passenger vehicles (Euro 2–Euro 4). Traditional single-ring aromatic precursors and naphthalene could explain 51–90 % of the formed SOA. Unspeciated species such as branched and cyclic alkanes might be the possible precursors for the unexplained SOA. A high-resolution time-of-flight aerosol mass spectrometer was used to characterize the chemical composition of SOA. The relationship between f_{43} (ratio of m/z 43, mostly $C_2H_3O^+$, to the total signal in mass spectrum) and f_{44} (mostly CO_2^+) of the gasoline vehicle exhaust SOA is similar to the ambient semi-volatile oxygenated organic aerosol (SV-OOA). We plot the O : C and H : C molar ratios of SOA in a Van Krevelen diagram. The slopes of ΔH : C/ΔO : C ranged from −0.59 to −0.36, suggesting that the oxidation chemistry in these experiments was a combination of carboxylic acid and alcohol/peroxide formation.

ACPD
15, 10553–10592, 2015

1 Introduction

The formation mechanisms, magnitude and chemical composition of airborne fine particulate matter ($PM_{2.5}$) are important to evaluate its effects on human health and climate (Hallquist et al., 2009). Organic aerosol (OA) contributes roughly ~ 20–50 % of the total fine particle mass at continental mid-latitudes (Saxena and Hildemann, 1996; Kanakidou et al., 2005). Atmospheric OA includes primary organic aerosol (POA) emitted from sources such as combustion of fossil fuels, biomass burning and volcanic eruptions, and secondary organic aerosol (SOA) formed via gas-particle conversion such as nucleation, condensation, and heterogeneous and multiphase chemistry or the aging of POA (Donahue et al., 2009; Jimenez et al., 2009). SOA is ubiquitous and dominates the total OA in various atmospheric environments, accounting for approximately two-thirds of the total OA in urban areas to almost 90 % in urban downwind and rural areas in Northern Hemisphere mid-latitudes (Zhang et al., 2007). China, for example, has serious air quality problem due to $PM_{2.5}$ pollution in the recent decade (Chan and Yao, 2008; Q. Zhang et al., 2012), and SOA had contributed 30–90 % of OA mass in its megacities (He et al., 2001; Cao et al., 2003; Duan et al., 2005, 2007; Yang et al., 2005; Hagler et al., 2006). However, models generally underestimate the observed OA levels mainly due to the unclear sources and formation processes of SOA (de Gouw et al., 2005; Heald et al., 2005; Johnson et al., 2006; Volkamer et al., 2006).

Vehicle exhausts emit plenty of primary PM and volatile organic compounds (VOCs) containing precursors of SOA, influencing the near-surface atmospheric chemistry and the air quality, especially in urban areas. SOA formation from diesel generators and vehicles has been widely studied in smog chambers, demonstrating that the SOA mass formed from the exhaust of diesel generators and medium-, and heavy-duty diesel vehicles (HDDVs) usually exceeds the mass of emitted POA (Robinson et al., 2007; Weitkamp et al., 2007; Chirico et al., 2010; Miracolo et al., 2010; Samy and Zielinska, 2010; Nakao et al., 2011; Kroll et al., 2012). However, there are few studies on the SOA formation from gasoline vehicle exhausts. Nordin et al. (2013) investigated

ACPD
15, 10553–10592, 2015

SOA formation from idling gasoline exhausts from three passenger vehicles (Euro 2–Euro 4), finding that C_6–C_9 light aromatics contributed up to 60 % of the formed SOA. While Platt et al. (2013) estimated aromatic precursors including C_6–C_{10} light aromatics and naphthalene were responsible for less than 20 % of the SOA formed from the aging of emissions from a Euro 5 gasoline car operated during a New European Driving Cycle. To exclude the influence of a small sample size, Gordon et al. (2014) studied aging of emissions from 15 light-duty gasoline vehicles with model years ranging from 1987 to 2011, concluding that traditional precursors could fully explain the SOA from oldest vehicles and unspeciated organics were responsible for the majority of the SOA from the newer vehicles. Therefore, chemical compositions of SOA formed from gasoline vehicle exhaust varied a lot among vehicles with different types, model years and operating conditions.

However, in China there is still no information on SOA formation from vehicle exhausts in the literature. The possession of LDGVs was 98.8 million in 2012 in China and increased at a rate of approximately 20 % per year since 2005 (NBSC, 2013). Furthermore, gasoline fuel in China has relatively higher mass content of alkenes and aromatic hydrocarbons than that in US (Schauer et al., 2002; Zhang et al., 2013), and current emission standards of LDGVs in China lag behind European countries and US. The emission factors of $PM_{2.5}$, organic carbon (OC), element carbon (EC), NO_x, SO_2, NH_3 and non-methane hydrocarbons (NMHCs) for on-road vehicles in China were quite different from those in other countries (Liu et al., 2014; Zhang et al., 2015). Therefore, it is urgent to investigate the SOA formation from vehicle exhaust in China to help make suitable policies to mitigate air pollution and also to provide valuable parameters to chemical transport models.

Here, we directly introduced dilute emissions from two idling light-duty gasoline vehicles (LDGVs) in China to a smog chamber to investigate the SOA formation. The magnitude and composition of the SOA formed from gasoline vehicle exhaust and whether traditional SOA precursors can explain the formed SOA was evaluated and discussed in this paper.

ACPD
15, 10553–10592, 2015

2 Materials and methods

2.1 Experimental setup

The photochemical aging experiments were carried out in the smog chamber in Guangzhou Institute of Geochemistry, Chinese Academy of Sciences (GIG-CAS). The GIG-CAS smog chamber has a 30 m^3 fluorinated ethylene propylene (FEP) reactor housed in a temperature-controlled room. Details of setup and facilities about the chamber have been described elsewhere (Wang et al., 2014). Briefly, black lamps (1.2 m-long, 60 W Philips/10R BL, Royal Dutch Philips Electronics Ltd, the Netherlands) are used as light source, providing a NO_2 photolysis rate of 0.49 min^{-1}. Two Teflon-coated fans are installed inside the reactor to guarantee well mixing of the introduced gas species and particles within 120 s. Temperature can be set in the range from −10 to 40 °C at accuracy of ±1 °C as measured by eight temperature sensors inside the enclosure and one just inside the reactor. Relative humidity (RH) inside the reactor is achieved by vaporizing Milli-Q ultrapure water contained in a 0.5 L Florence flask and then flushing the water vapor into the reactor with purified dry air until target RH is reached. In the present study, temperature and RH inside the reactor were all set to 25 °C and 50 %, respectively. During the experiments, the top frame is automatically lowered to maintain a differential positive pressure inside the reactor against the enclosure to avoid the contamination of the enclosure air.

Gasoline vehicle exhausts were injected to the reactor through Teflon lines using two oil-free pumps (Gast Manufacturing, Inc, USA) at a flow rate of 40 L min^{-1}. The injection time varied from a few minutes to more than one hour based on the primary emissions of different vehicles. A schematic of the smog chamber and the vehicle exhaust injection system is shown in Fig. 1.

ACPD
15, 10553–10592, 2015

2.2 Characterization of gas- and particle-phase chemical compositions and particle sizes

Gas-phase ozone (O_3) and NO_x were measured online with dedicated monitors (EC9810 and 9841T, Ecotech, Australia). Online monitoring of parent NMHCs such as C_6–C_{10} single-ring aromatic hydrocarbons and their oxidation products were available with a commercial proton-transfer-reaction time-of-flight mass spectrometer (PTR-TOF-MS, Model 2000, Ionicon Analytik GmbH, Austria). Detailed descriptions of the PTR-TOF-MS technique can be found elsewhere (Lindinger et al., 1998; Jordan et al., 2009). In this study the decay curve of toluene measured by PTR-TOF-MS was also used to derive the average hydroxyl radical (OH) concentration during each experiment. A wide spectrum of VOCs were also measured offline by drawing 250 mL air inside the reactor to a Model 7100 Preconcentrator (Entech Instruments Inc., USA) coupled with an Agilent 5973N gas chromatography-mass selective detector/flame ionization detector/electron capture detector (GC-MSD/FID/ECD, Agilent Technologies, USA). Detailed descriptions of the method can be found elsewhere (Wang and Wu, 2008; Y. Zhang et al., 2010, 2012, 2013). The VOC concentrations measured offline were also used as an independent check of that measured online by the PTR-TOF-MS. To determine CO/CO_2 concentrations before and after the introduction of exhausts, air samples were also collected into 2 L cleaned Teflon bags. CO was analyzed using a gas chromatography (Agilent 6980GC, USA) with a flame ionization detector and a packed column (5A Molecular Sieve 60/80 mesh, 3 m $\times$1/8 inch) (Y. Zhang et al., 2012), and CO_2 was analyzed with a HP 4890D gas chromatography (Yi et al., 2007). The detection limits of CO and CO_2 were < 30 ppb. The relative SDs were all less than 3 % based on 7 duplicates running 1.0 ppm CO and CO_2 standards (Spectra Gases Inc, USA).

A high-resolution time-of-flight aerosol mass spectrometer (HR-TOF-MS, Aerodyne Research Incorporated, USA) was used to measure the particle chemical compositions (Jayne et al., 2000; DeCarlo et al., 2006). The instrument was operated in the high sensitivity V-mode and high resolution W-mode alternatively every two minutes.

ACPD
15, 10553–10592, 2015

The toolkit Squirrel 1.51H was used to obtain time series of various mass components (sulfate, nitrate, ammonium and organics). We used the toolkit Pika 1.1H to determine the average element ratios of organics, like H : C, O : C, and N : C (Aiken et al., 2007, 2008). The contribution of gas-phase CO_2 to the m/z 44 signal was corrected using the measured CO_2 concentrations. The HR-TOF-MS was calibrated using 300 nm monodisperse ammonium nitrate particles.

Particle number/volume concentrations and size distributions were measured with a scanning mobility particle sizer (SMPS, TSI Incorporated, USA, classifier model 3080, CPC model 3775). Flow rates of sheath and aerosol flow were 3.0 and 0.3 L min^{-1}, respectively, allowing a size distribution scanning ranging from 14 to 700 nm within 255 s. The accuracy of the particle number concentration is ±10 %. An aerosol density of 1.4 g cm^{-3} was assumed to convert the particle volume concentration into the mass concentration (Zhang et al., 2005).

2.3 Experimental procedure

Two light-duty gasoline-powered vehicles were used in this study, one Euro 1 and one Euro 4 vehicles. They are both port fuel injected vehicles. More details of the vehicles are listed in Table 1. Both of the vehicles were fueled with Grade 93# gasoline, which complies with the Euro III gasoline fuel standard. Details of the oil compositions can be found in our previous study (Zhang et al., 2013).

Prior to each experiment, the reactor was evacuated and filled with purified dry air for at least 5 times, then the reactor was flushed with purified dry air for at least 48 h until no residual hydrocarbons, O_3, NO_x, or particles were detected in the reactor to avoid carry-over problems from day-to-day experiments. Prior to the introduction of exhaust, the temperature control system and Teflon coated fans were turned on. The exhaust could be injected when the temperature in the reactor was stable at the set temperature 25 °C.

The LDGV was parked outside the laboratory and tested at idling. Before the injection of exhaust, the cars were at idling for at least half an hour to warm up the three-

ACPD
15, 10553–10592, 2015

way catalysts, and then the vehicle exhausts were injected into the reactor. During the introduction, the raw exhausts were also sampled into 8 L cleaned aluminum foil bags by a mechanical pump with a flow rate of about 5 L min^{-1}. VOCs in these samples were measured offline by the same method mentioned above. The exhaust in the reactor was diluted by a factor of 13–30 compared to the tailpipe.

Additional NO was then added to adjust the VOC/NO_x ratios to around 10.0 or 2.0 (Table 2), within the range of 0.5–10 reported in gasoline vehicle exhaust tests and downwind urban areas (Clairotte et al., 2013). The initial concentrations of NO_x at the start of the experiments ranged from 134 to 956 ppb. In each experiment CH_3CN was used as an indicator of dilution in the reactor. After being characterized in the dark for more than 30 min, the exhaust was exposed to black light continuously for 5 h. After the black lamps were switched off, the formed SOA was characterized for another 2 to 3 h to correct the particles wall loss.

2.4 Data analysis

2.4.1 Wall loss corrections

The loss of particles and organic vapors to the reactor walls has to be accounted for to accurately quantify the SOA formation. The loss of particles onto the walls has been well constrained and is treated as a first-order process (McMurry and Grosjean, 1985). The wall-loss rate constant was determined separately for each experiment by fitting the SMPS and AMS data when no new particles were formed. By applying this rate to the entire experiment, we use the same method as Pathak et al. (2007) treating the particle wall loss as a first order process to correct the wall loss of the particles. The wall loss of particles is a size-dependent process, therefore, the influence of nucleation need to be examined due to the rapid loss of nucleation mode particles. In this study, the impact of the nucleation event on wall-loss estimate is considered to be negligible for only less than 3 % of the particle mass is in the nucleation mode ten minutes after nucleation for all the experiments (Fig. 2). In general, the loss of

ACPD
15, 10553–10592, 2015

condensable organic vapors to the walls is estimated for two limiting cases (Weitkamp et al., 2007; Hildebrandt et al., 2009). In the first case (designated $\omega = 0$), no organic vapors is lost to the walls (only to suspended particles). In the second case (designated $\omega = 1$), the particles on the walls are in equilibrium with the organic vapors; therefore condensation to the particles on the walls is identical to the suspended particles. We use the $\omega = 0$ wall-loss correction assuming the organic vapors only condensation onto suspended particles. The $\omega = 1$ wall-loss correction is not suitable for the experiments here in which nucleation occurred and no seed particles were added (Henry et al., 2012).

2.4.2 AMS data corrections

Theoretically, the sum of the PM mass measured by AMS should be equal to the mass calculated from the SMPS mass size distributions. However, both the two methods have limitations. One must assume a particle shape and density to convert the volume concentration measured by SMPS to the mass concentration. Here, we assume that particles are spherical with an average density of $1.4\,\mathrm{g\,cm^{-3}}$ (Zhang et al., 2005). Fractal-like particles will cause the overestimate of the spherical equivalent diameter, thus overestimating the particle mass. AMS tends to underestimate the PM mass due to the AMS collection efficiency (Gordon et al., 2014), leading to the discrepancy between the AMS data and SMPS data. In this study, we use the same method as Gordon et al. (2014) to correct the AMS data.

For all the experiments with discrepancies between the AMS and SMPS data (Fig. 3), we assume that the difference in mass has the same composition as the measured components. We then calculate scaling factors, $\mathrm{AMS_{sf}}$, to correct the PM mass measured by AMS and make it accordant with the SMPS measurements. The scaling factor is

$$\mathrm{AMS_{sf}} = \frac{C_{\mathrm{SMPS}}}{C_{\mathrm{Org}} + C_{\mathrm{SO_4}} + C_{\mathrm{NO_3}} + C_{\mathrm{NH_4}}} \quad (1)$$

ACPD
15, 10553–10592, 2015

where C_{SMPS} is the total particle mass concentration derived by the SMPS, C_{Org}, C_{SO_4}, C_{NO_3} and C_{NH_4} are the mass concentrations of organics, sulfate, nitrate and ammonium measured by the AMS. The AMS_{sf} for each time step after nucleation is calculated and used to scale the AMS data for the entire experiment.

2.4.3 Effective SOA yields

To compare the SOA formation with other studies, we calculated effective SOA yields for all experiments. The effective SOA yield Y was defined as the ratio of the wall-loss-corrected SOA mass to the mass of reacted organic precursors (Odum et al., 1996, 1997; Donahue et al., 2006). In this study, reacted organic precursors included in calculation are only those quantified by GC-MSD, including benzene, toluene, C2-benzene, C3-benzene, C4-benzene and naphthalene. A detailed list of these compounds is presented in Table 3. At the beginning and end of each experiment, simulating air in the reactor were collected into evacuated 2 L stainless steel canisters and analyzed by GC-MSD to determine the mass of reacted organic precursors.

2.4.4 Emission factors

Emission factor (EF) of a pollutant P is calculated on a fuel basis ($g\,kg^{-1}$):

$$EF = 10^3 \cdot [\Delta P] \cdot \left(\frac{MW_{CO_2}}{[\Delta CO_2]} + \frac{MW_{CO}}{[\Delta CO]} + \frac{MW_{HC}}{[\Delta HC]} \right) \cdot \frac{\omega_C}{MW_C} \quad (2)$$

where $[\Delta P]$, $[\Delta CO_2]$, $[\Delta CO]$, and $[\Delta HC]$ are the background corrected concentrations of P, CO_2, CO and the total hydrocarbons in the reactor in $\mu g\,m^{-3}$; MW_{CO_2}, MW_{CO}, MW_{HC}, and MW_C are the molecular weights of CO_2, CO, HC and C. ω_C (0.85) is the carbon intensity of the gasoline (Kirchstetter et al., 1999).

ACPD
15, 10553–10592, 2015

3 Results and discussion

3.1 VOC composition

Figure 4 shows the average composition of gasoline vehicle exhausts from vehicle I (Euro 4) and II (Euro 1). For vehicle I and II, alkanes shared about 42.9 and 66.2 % of the total speciated NMHCs measured with the GC-FID/MSD by mass, respectively, dominating the NMHCs emissions in gasoline vehicle exhausts. Due to the high concentrations of isopentane and methylpentane, branched alkanes contributed approximately 44.9 % of the total NMHCs for vehicle II, quite higher than that for vehicle I (23.3 %). Aromatic hydrocarbons accounted for about 38.0 and 22.5 % of the total NMHCs for vehicle I and II, respectively, relatively higher than 10–15 % observed by Nordin et al. (2013) for Euro 2, 3 and 4 vehicles. The variations of the composition of LDGV exhausts may be due to the difference of the fuel, vehicle type and emission standard.

The averaged emission factors of NMHCs and aromatic hydrocarbons for vehicle I were 2.1 and 0.8 $g\,kg^{-1}$, approximately 1.3 and 0.5 times lower than those for vehicle II, respectively. Compared with a Euro 5 gasoline vehicle operated during a New European Driving Cycle, the emission factor of NMHCs for vehicle I was about 1.7 times higher (Platt et al., 2013). There is a clear reduction of primary emissions from vehicles with stricter emission standards. It is worth noting that emissions of HC from gasoline vehicles during idling were observed to be lower than those in the acceleration and deceleration modes (Tong et al., 2000; Yamamoto et al., 2012; Huang et al., 2013), but in a similar level with those in the cruising mode (Tong et al., 2000).

3.2 SOA formation

Figure 5 shows the temporal evolution of gas-phase and particle-phase species during a typical smog chamber experiment. During −1.3 to −0.85 h, the vehicle exhausts were introduced into the reactor. At time = −0.55 h, the relative humidity was adjusted to ap-

ACPD
15, 10553–10592, 2015

proximately 40 %, and HR-TOF-AMS was connected to characterize the primary PM. NO was injected to adjust the VOC/NO_x ratio at approximately time = −0.25 h. After the black lamps were turned on, NO was fast converted to NO_2 in less than 1 h, and then O_3 was accumulated and OH radical was formed. When NO concentration decreased to a low level about 5 ppb, gas-phase light aromatics especially C_3–benzene with higher reactivity, decayed rapidly due to the reaction with OH radical. SOA was thus rapidly formed and increased to a high level in less than 2 h. As shown in Table 4, at the end of all the experiments, the formed SOA was 12–259 times as high as POA. This enhancement is consistent with 9–500 recently reported by Nordin et al. (2013) when studying SOA formation from idling European gasoline passenger vehicle emissions. As shown in Fig. 5c, the total particle number concentration increased fast from 82 to 116 143 cm^{-3} in approximately 10 min, indicating dramatic new particle formation. After nucleation occured, the mean diameter increased from 20 to 60 nm in about 1.5 h. Because particles with diameters lager than 50 nm can act as cloud condensation nuclei (CCN) (McFiggans et al., 2006) and influence the radiative forcing, SOA from vehicle exhausts may has climate effects to a certain extent as well as air quality effects.

SOA production factors (PF) for LDGVs in China were estimated to vary from 0.001 to 0.044 g kg^{-1} fuel, which are within the results of Nordin et al. (2013) and Gordon et al. (2014) with OH exposure around 5.0×10^6 molecules cm^{-3} h. A recent study investigating SOA formation from in-use vehicle emissions in a highway tunnel in Pittsburg indicated that the peak SOA production was measured at an OH exposure of 1.9×10^8 molecules cm^{-3} h and current smog chamber studies may underestimate the ultimate SOA production by a maximum factor of about 10 due to the limited OH exposure (Tkacik et al., 2014). Decay of toluene measured by PTR-TOF-MS is used to derive the average OH concentration during each experiment. Changes in the toluene concentration over time can be expressed as:

$$\frac{\mathrm{d[toluene]}}{\mathrm{d}t} = -k \cdot [\mathrm{OH}] \cdot [\mathrm{toluene}] \quad (3)$$

ACPD
15, 10553–10592, 2015

where k is the reaction rate constant between toluene and OH radical. Assuming a constant OH concentration during an experiment, we can integrate Eq. (3) to get Eq. (4):

$$\ln\left(\frac{[\text{toluene}]_0}{[\text{toluene}]_t}\right) = k \cdot [\text{OH}] \cdot t \quad (4)$$

By plotting the natural logarithm (ln) of the ratio between the initial toluene concentration and the toluene concentration at time t vs. time, we can obtain a slope that equals $k \cdot [\text{OH}]$. The average OH concentration is therefore:

$$[\text{OH}] = \frac{\text{slope}}{k} \quad (5)$$

The average OH radical concentration (Table 4) was determined to be 0.79–1.23 × 10^6 molecules cm^{-3} during our experiments. This OH level was about ten times lower than the average OH concentration of 1.5 × 10^7 molecules cm^{-3} around noon in summer in the Pearl River Delta, China (Hofzumahaus et al., 2009). The OH exposure in this study is only 5 × 10^6 molecules cm^{-3} h, equivalent to 0.3 h of atmospheric oxidation. Therefore, the real-world SOA production factor from LDGVs in the atmosphere in China may be even higher than our estimation.

3.3 SOA yield

Effective SOA yield from vehicle exhaust calculated as described in 2.4.3 ranged from 2.8 to 17.2 %. Pankow (1994a, b) and Odum et al. (1996) indicated that Y is a function of M_0 and the relation is described as:

$$Y = M_0 \sum\left(\frac{\alpha_i K_{\text{om},i}}{1 + K_{\text{om},i} M_0}\right) \quad (6)$$

where $K_{\text{om},i}$ and α_i are the mass-based absorption equilibrium partitioning coefficient and stoichiometric coefficient of product i, respectively; M_0 is the total mass concentration of organic material.

ACPD
15, 10553–10592, 2015

Comparison of effective yield data obtained for the LDGV exhaust in this study with those of Nordin et al. (2013) is shown in Fig. 6. Effective yield data of this study are well fit with the one-product model, namely $Y = M_0 \left(\frac{\alpha_1 K_{om,1}}{1+K_{om,1} M_0} \right)$. The appropriate values for α_1 and $K_{om,1}$ when fitting the yields are 0.350 ± 0.114 and 0.007 ± 0.004, respectively. Compared with the study of Nordin et al. (2013), the effective SOA yield in this study were relatively lower when the M_0 is equal. Ammonium sulfate was added as the seed aerosol by Nordin et al. (2013). Previous studies showed that SOA yields from the photooxidation of aromatics hydrocarbons were lower without the presence of inorganic seed particles (Kroll et al., 2007; Lu et al., 2009). The average OH concentration is relatively lower than that in the study of Nordin et al. (2013). Ng et al. (2007) indicated that faster oxidation rates caused by higher OH concentrations would result in higher SOA yields. Additionally, the different VOCs profiles of exhausts might also influence the SOA yields.

SOA production from the reacted organic precursors can be estimated by the following formula:

$$\Delta \mathrm{SOA}_{\mathrm{predicted}} = \sum_j \left(\Delta X_j \times Y_j \right) \quad (7)$$

where $\Delta \mathrm{SOA}_{\mathrm{predicted}}$ is the predicted SOA concentration in $\mu g\,m^{-3}$; ΔX_j is the mass of reacted aromatic hydrocarbon X_j in $\mu g\,m^{-3}$; and Y_j is the corresponding SOA yield of X_j. In this study, the SOA yield of benzene and other single-ring aromatics were estimated using the two-product model curves taken from Borrás et al. (2012) and Odum et al. (1997), respectively. While the SOA yield of naphthalene was taken from Shakya et al. (2010). The aerosol yield curves from literature were converted to the same aerosol density of $1.4\,g\,cm^{-3}$ as this study. The SOA yield for each precursor was calculated for the measured concentration of OA in the reactor. Then the predicted SOA production from each precursor can be calculated (Table 3).

Figure 7 shows the contributions of the predicted benzene SOA, toluene SOA, C_2–benzene SOA, C_3–benzene SOA, C_4–benzene SOA and naphthalene SOA to the total

ACPD
15, 10553–10592, 2015

measured SOA in all experiments. C_4–benzene contributed negligible SOA because of the very low emissions of C_4–benzene from light-duty gasoline vehicles (Table 5). Though benzene took relatively higher percentage of the total NMHCs, benzene also accounted for a negligible proportion of the formed SOA due to its low reactivity with OH radicals. Naphthalene was previously estimated to contribute around 5 % of the vehicle SOA mass (Nordin et al., 2013). While in this study naphthalene was calculated to contribute 8–52 % of the formed SOA. The initial concentrations of naphthalene in this study ranged from 8.5 to 39.5 ppb, much higher than 2.8–4.4 ppb in the study of Nordin et al. (2013). The high contributions of naphthalene are probably attributed to its relatively higher initial concentrations and higher mass yield than single-ring aromatics for similar experimental conditions (Odum et al., 1997; Ng et al., 2007).

Totally, single-ring aromatics and naphthalene accounted for 51–90 % of the measured SOA, comparable to the estimation that classical C6–C9 light aromatics were responsible for 60 % of the formed SOA from gasoline vehicle exhausts (Nordin et al., 2013), indicating that there are other SOA precursors in the LDGV exhausts. Platt et al. (2013) attributed the unexplained SOA formed from the aging of emissions from a Euro 5 gasoline car to highly oxygenated hydrocarbons. In addition, intermediate-volatility organic compounds (IVOCs) such as branched and cyclic alkanes were recognized as important SOA precursors derived from wood burning, diesel engine and aircraft exhaust (Robinson et al., 2007; Weitkamp et al., 2007; Grieshop et al., 2009; Tkacik et al., 2012). Gordon et al. (2014) found that unspeciated species including branched and cyclic alkanes contributed about 30 % of the nonmethane organic gas emissions from LDGVs with model years of 1995 or later and be associated with the majority of the SOA formation. Tkacik et al. (2014) also found that unspeciated species were predicted to contribute twice as much SOA from in-use vehicle emissions as traditional precursors. It is worth noting that photooxidation of aromatic hydrocarbons in a complex mixture such as gasoline vehicle exhausts might alter the SOA yield compared to pure precursor experiments, thus probably influencing the estimation in this study (Song et al., 2007).

ACPD
15, 10553–10592, 2015

3.4 SOA composition

Fragmentations derived from the AMS data have been widely used to explore the oxidation degree of the organic aerosols (Zhang et al., 2005; Ng et al., 2010; Heald et al., 2010). The usually used ion fragments include m/z 43, 44 and 57. The dominating organic peaks in gasoline vehicle exhaust SOA are m/z 43 and 44 (Nordin et al., 2013), while m/z 57 is a main hydrocarbon fragment in diesel SOA (Chirico et al., 2010). Here, we use the approach of Ng et al. (2010) by plotting the fractions of total organic signal at m/z 43 (f_{43}) vs. m/z 44 (f_{44}) together with the triangle defined according to the analysis of ambient AMS data. The m/z 43 signal includes $C_3H_7^+$ and $C_2H_3O^+$ ions, indicating fresh less oxidized organic aerosols. The m/z 44 signal, dominated by CO_2^+ and formed from the thermal decarboxylation of organic acids, is an indicator of highly oxygenated organic aerosols (Ng et al., 2010).

Figure 8a shows the f_{43} vs. f_{44} at the end of each experiment and the results of Nordin et al. (2013) and Presto et al. (2014), together with the triangle developed by Ng et al. (2010). The ambient low-volatility oxygenated OA (LV-OOA) and semi-volatile OOA (SV-OOA) factors fall in the upper and lower portions of the triangle, respectively. Our data mainly lie in the SV-OOA region, similar to the results of Nordin et al. (2013) and Presto et al. (2014). However, SOA in one experiment show relatively lower oxidation degree. This phenomenon reflects the different SOA compositions among different experiments and might be caused by the different VOCs profiles, OH exposure and organic mass loadings (Ng et al., 2010).

The O : C ratio can also be used to characterize the oxidation degree of the organic aerosols. After 5 h irradiation the H : C ratios varied from 1.22 to 1.37 and the O : C ratios from 0.43 to 0.69 for all the experiments. Almost all the O : C values were lower than 0.6, comparable to the SV-OOA compounds, which typically has O : C ratios between 0.3 and 0.6 (Jimenez et al., 2009). Platt et al. (2013) observed a relatively higher O : C ratio of 0.7 on the aging (OH = 12×10^6 molecules cm^{-3} h) of emissions from a Euro 5 gasoline car operated during a New European Driving Cycle. As a higher OH exposure

ACPD
15, 10553–10592, 2015

will lead to a higher O : C ratio, if the gasoline exhaust in this study was irradiated under a similar OH exposure to that of Platt et al. (2013), the O : C ratios might reach to the similar level or higher, comparable to the LV-OOA factor (Jimenez et al., 2009).

In Fig. 8b we plot the O : C and H : C molar ratios after SOA was formed during experiments 1, 2 and 3 on a Van Krevelen diagram (Heald et al., 2010). The slopes ranged from −0.59 to −0.36, similar to previous laboratory studies of Tkacik et al. (2012) for cyclic, linear and branched alkanes, Jathar et al. (2013) for unburned fuel and Presto et al. (2014) for light-duty gasoline vehicle exhaust. They are also similar to the ambient data (Ng et al., 2011). A slope of −1, −0.5 and 0 in the Van Krevelen diagram represents the addition of alcohol/peroxide, the addition of carboxylic acid with fragmentation, and the addition of carboxylic acid without fragmentation, respectively (Heald et al., 2010; Ng et al., 2011). Consequently, the slopes in this study indicate that the SOA formation is a combination of the addition of both carboxylic acid and alcohol/peroxide function groups without C-C bond cleavage and/or the addition of carboxylic acid with C-C bond breakage (Heald et al., 2010; Ng et al., 2011).

4 Conclusion

Better understanding of the magnitude and property of SOA formed from exhausts of vehicles in China will provide valuable information to the government and climate modelers. As presented in this study, gasoline vehicle exhaust SOA was fast formed and extremely exceeded the POA. Traditional single-ring aromatic precursors and naphthalene could explain 51–90 % of the formed SOA. Unspeciated species such as branched and cyclic alkanes might be the possible precursors for the unexplained SOA. More work is needed to better understand the role of LDGVs on the fossil SOA in the atmosphere by studying the SOA formation of emissions from more vehicles with different model years, types and emission standards. Furthermore, given that the emissions from gasoline vehicles vary a lot with the driving conditions, the SOA formation of emis-

ACPD
15, 10553–10592, 2015

sions from LDGVs in China under "real world" conditions is needed to be investigated in the future.

Acknowledgements. This study was supported by National Natural Science Foundation of China (Project No. 41025012/41121063), Strategic Priority Research Program of the Chinese Academy of Sciences (Grant No. XDB05010200), NSFC-Guangdong Joint Funds (U0833003) and Guangzhou Institute of Geochemistry (GIGCAS 135 project Y234161001).

References

Aiken, A. C., DeCarlo, P. F., and Jimenez, J. L.: Elemental analysis of organic species with electron ionization high-resolution mass spectrometry, Anal. Chem., 79, 8350–8358, doi:10.1021/ac071150w, 2007.

Aiken, A. C., DeCarlo, P. F., Kroll, J. H., Worsnop, D. R., Huffman, J. A., Docherty, K. S., Ulbrich, I. M., Mohr, C., Kimmel, J. R., Sueper, D., Sun, Y., Zhang, Q., Trimborn, A., Northway, M., Ziemann, P. J., Canagaratna, M. R., Onasch, T. B., Alfarra, M. R., Prevot, A. S. H., Dommen, J., Duplissy, J., Metzger, A., Baltensperger, U., and Jimenez, J. L.: O/C and OM/OC ratios of primary, secondary, and ambient organic aerosols with high-resolution time-of-flight aerosol mass spectrometry, Environ. Sci. Technol., 42, 4478–4485, doi:10.1021/es703009q, 2008.

Borrás, E. and Tortajada-Genaro, L. A.: Secondary organic aerosol formation from the photo-oxidation of benzene, Atmos. Environ., 47, 154–163, 2012.

Cao, J. J., Lee, S. C., Ho, K. F., Zhang, X. Y., Zou, S. C., Fung, K., Chow, J. C., and Watson, J. G.: Characteristics of carbonaceous aerosol in Pearl River Delta Region, China during 2001 winter period, Atmos. Environ., 37, 1451–1460, doi:10.1016/S1352-2310(02)01002-6, 2003.

Chan, C. K. and Yao, X.: Air pollution in mega cities in China, Atmos. Environ., 42, 1–42, doi:10.1016/j.atmosenv.2007.09.003, 2008.

Chirico, R., DeCarlo, P. F., Heringa, M. F., Tritscher, T., Richter, R., Prévôt, A. S. H., Dommen, J., Weingartner, E., Wehrle, G., Gysel, M., Laborde, M., and Baltensperger, U.: Impact of aftertreatment devices on primary emissions and secondary organic aerosol formation potential from in-use diesel vehicles: results from smog chamber experiments, Atmos. Chem. Phys., 10, 11545–11563, doi:10.5194/acp-10-11545-2010, 2010.

ACPD
15, 10553–10592, 2015

Clairotte, M., Adam, T. W., Zardini, A. A., Manfredi, U., Martini, G., Krasenbrink, A., Vicet, A., Tournie, E., and Astorga, C.: Effects of low temperature on the cold start gaseous emissions from light duty vehicles fuelled by ethanol-blended gasoline, Appl. Energ., 102, 44–54, 2013.

DeCarlo, P. F., Kimmel, J. R., Trimborn, A., Northway, M. J., Jayne, J. T., Aiken, A. C., Gonin, M., Fuhrer, K., Horvath, T., Docherty, K. S., Worsnop, D. R., and Jimenez, J. L.: Field-deployable, high-resolution, time-of-flight aerosol mass spectrometer, Anal. Chem., 78, 8281–8289, doi:10.1021/ac061249n, 2006.

de Gouw, J. A., Middlebrook, A. M., Warneke, C., Goldan, P. D., Kuster, W. C., Roberts, J. M., Fehsenfeld, F. C., Worsnop, D. R., Canagaratna, M. R., Pszenny, A. A. P., Keene, W. C., Marchewka, M., Bertman, S. B., and Bates, T. S.: Budget of organic carbon in a polluted atmosphere: results from the New England Air Quality Study in 2002, J. Geophys. Res., 110, D16305, doi:10.1029/2004JD005623, 2005.

Donahue, N. M., Robinson, A. L., Stanier, C. O., and Pandis, S. N.: Coupled partitioning, dilution, and chemical aging of semivolatile organics, Environ. Sci. Technol., 40, 2635–2643, doi:10.1021/es052297c, 2006.

Donahue, N. M., Robinson, A. L., and Pandis, S. N.: Atmospheric organic particulate matter: from smoke to secondary organic aerosol, Atmos. Environ., 43, 94–106, doi:10.1016/j.atmosenv.2008.09.055, 2009.

Duan, F. K., He, K. B., Ma, Y. L., Jia, Y. T., Yang, F. M., Lei, Y., Tanaka, S., and Okuta, T.: Characteristics of carbonaceous aerosols in Beijing, China, Chemosphere, 60, 355–364, doi:10.1016/j.chemosphere.2004.12.035, 2005.

Duan, F. K., Liu, X. D., He, K. B., Li, Y. W., and Dong, S. P.: Characteristics and source identification of particulate matter in wintertime in Beijing, Water Air Soil Poll., 180, 171–183, doi:10.1007/s11270-006-9261-4, 2007.

Gordon, T. D., Presto, A. A., May, A. A., Nguyen, N. T., Lipsky, E. M., Donahue, N. M., Gutierrez, A., Zhang, M., Maddox, C., Rieger, P., Chattopadhyay, S., Maldonado, H., Maricq, M. M., and Robinson, A. L.: Secondary organic aerosol formation exceeds primary particulate matter emissions for light-duty gasoline vehicles, Atmos. Chem. Phys., 14, 4661–4678, doi:10.5194/acp-14-4661-2014, 2014.

Hagler, G. S., Bergin, M. H., Salmon, L. G., Yu, J. Z., Wan, E. C. H., Zheng, M., Zeng, L. M., Kiang, C. S., Zhang, Y. H., Lau, A. K. H., and Schauer, J. J.: Source areas and chemical composition of fine particulate matter in the Pearl River Delta region of China, Atmos. Environ., 40, 3802–3815, doi:10.1016/j.atmosenv.2006.02.032, 2006.

ACPD
15, 10553–10592, 2015

Hallquist, M., Wenger, J. C., Baltensperger, U., Rudich, Y., Simpson, D., Claeys, M., Dommen, J., Donahue, N. M., George, C., Goldstein, A. H., Hamilton, J. F., Herrmann, H., Hoffmann, T., Iinuma, Y., Jang, M., Jenkin, M. E., Jimenez, J. L., Kiendler-Scharr, A., Maenhaut, W., McFiggans, G., Mentel, Th. F., Monod, A., Prévôt, A. S. H., Seinfeld, J. H., Surratt, J. D., Szmigielski, R., and Wildt, J.: The formation, properties and impact of secondary organic aerosol: current and emerging issues, Atmos. Chem. Phys., 9, 5155–5236, doi:10.5194/acp-9-5155-2009, 2009.

He, K., Yang, F., Ma, Y., Zhang, Q., Yao, X., Chan, C. K., Cadle, S., Chan, T., and Mulawa, P.: The characteristics of $PM_{2.5}$ in Beijing, China, Atmos. Environ., 35, 4959–4970, doi:10.1016/S1352-2310(01)00301-6, 2001.

Heald, C. L., Jacob, D. J., Park, R. J., Russell, L. M., Huebert, B. J., Seinfeld, J. H., Liao, H., and Weber, R. J.: A large organic aerosol source in the free troposphere missing from current models, Geophys. Res. Lett., 32, L18809, doi:10.1029/2005GL023831, 2005.

Heald, C. L., Kroll, J. H., Jimenez, J. L., Docherty, K. S., DeCarlo, P. F., Aiken, A. C., Chen, Q., Martin, S. T., Farmer, D. K., and Artaxo, P.: A simplified description of the evolution of organic aerosol composition in the atmosphere, Geophys. Res. Lett., 37, L08803, doi:10.1029/2010gl042737, 2010.

Henry, K. M., Lohaus, T., and Donahue, N. M.: Organic Aerosol Yields from α-Pinene Oxidation: Bridging the Gap between First-Generation Yields and Aging Chemistry, Environ. Sci. Technol., 46, 12347–12354, doi:10.1021/es302060y, 2012.

Hildebrandt, L., Donahue, N. M., and Pandis, S. N.: High formation of secondary organic aerosol from the photo-oxidation of toluene, Atmos. Chem. Phys., 9, 2973–2986, doi:10.5194/acp-9-2973-2009, 2009.

Hofzumahaus, A., Rohrer, F., Lu, K., Bohn, B., Brauers, T., Chang, C.-C., Fuchs, H., Holland, F., Kita, K., Kondo, Y., Li, X., Lou, S., Shao, M., Zeng, L., Wahner, A., and Zhang, Y.: Amplified trace gas removal in the troposphere, Science, 324, 1702–1704, doi:10.1126/science.1164566, 2009.

Huang, C., Lou, D. M., Hu, Z. Y., Feng, Q., Chen, Y. R., Chen, C. H., Tan, P. Q., and Yao, D.: A PEMS study of the emissions of gaseous pollutants and ultrafine particles from gasoline- and diesel-fueled vehicles, Atmos. Environ., 77, 703–710, doi:10.1016/j.atmosenv.2013.05.059, 2013.

Jathar, S. H., Miracolo, M. A., Tkacik, D. S., Donahue, N. M., Adams, P. J., and Robinson, A. L.: Secondary Organic Aerosol Formation from Photo-Oxidation of Unburned Fuel: Experimen-

ACPD
15, 10553–10592, 2015

tal Results and Implications for Aerosol Formation from Combustion Emissions, Environ. Sci. Technol., 47, 12886–12893, doi:10.1021/es403445q, 2013.
Jathar, S. H., Gordon, T. D., Hennigan, C. J., Pye, H. O. T., Pouliot, G., Adams, P. J., Donahue, N. M., and Robinson, A. L.: Unspeciated organic emissions from combustion sources and their influence on the secondary organic aerosol budget in the United States, P. Natl. Acad. Sci. USA, 111, 10473–10478, doi:10.1073/pnas.1323740111, 2014.
Jayne, J. T., Leard, D. C., Zhang, X., Davidovits, P., Smith, K. A., Kolb, C. E., and Worsnop, D. R.: Development of an aerosol mass spectrometer for size and composition analysis of submicron particles, Aerosol. Sci. Tech., 33, 49–70, doi:10.1080/027868200410840, 2000.
Jimenez, J. L., Canagaratna, M. R., Donahue, N. M., Prevot, A. S. H., Zhang, Q., Kroll, J. H., DeCarlo, P. F., Allan, J. D., Coe, H., Ng, N. L., Aiken, A. C., Docherty, K. S., Ulbrich, I. M., Grieshop, A. P., Robinson, A. L., Duplissy, J., Smith, J. D., Wilson, K. R., Lanz, V. A., Hueglin, C., Sun, Y. L., Tian, J., Laaksonen, A., Raatikainen, T., Rautiainen, J., Vaattovaara, P., Ehn, M., Kulmala, M., Tomlinson, J. M., Collins, D. R., Cubison, M. J. E., Dunlea, J., Huffman, J. A., Onasch, T. B., Alfarra, M. R., Williams, P. I., Bower, K., Kondo, Y., Schneider, J., Drewnick, F., Borrmann, S., Weimer, S., Demerjian, K., Salcedo, D., Cottrell, L., Griffin, R., Takami, A., Miyoshi, T., Hatakeyama, S., Shimono, A., Sun, J. Y., Zhang, Y. M., Dzepina, K., Kimmel, J. R., Sueper, D., Jayne, J. T., Herndon, S. C., Trimborn, A. M., Williams, L. R., Wood, E. C., Middlebrook, A. M., Kolb, C. E., Baltensperger, U., and Worsnop, D. R.: Evolution of organic aerosols in the atmosphere, Science, 326, 1525–1529, doi:10.1126/science.1180353, 2009.
Johnson, D., Utembe, S. R., Jenkin, M. E., Derwent, R. G., Hayman, G. D., Alfarra, M. R., Coe, H., and McFiggans, G.: Simulating regional scale secondary organic aerosol formation during the TORCH 2003 campaign in the southern UK, Atmos. Chem. Phys., 6, 403–418, doi:10.5194/acp-6-403-2006, 2006.
Jordan, A., Haidacher, S., Hanel, G., Hartungen, E., Mark, L., Seehauser, H., Schottkowsky, R., Sulzer, P., and Mark, T. D.: A high resolution and high sensitivity proton-transfer-reaction time-of-flight mass spectrometer (PTR-TOF-MS), Int. J. Mass Spectrom., 286, 122–128, 2009.
Kanakidou, M., Seinfeld, J. H., Pandis, S. N., Barnes, I., Dentener, F. J., Facchini, M. C., Van Dingenen, R., Ervens, B., Nenes, A., Nielsen, C. J., Swietlicki, E., Putaud, J. P., Balkanski, Y., Fuzzi, S., Horth, J., Moortgat, G. K., Winterhalter, R., Myhre, C. E. L., Tsigaridis, K., Vignati, E., Stephanou, E. G., and Wilson, J.: Organic aerosol and global climate modelling: a review, Atmos. Chem. Phys., 5, 1053–1123, doi:10.5194/acp-5-1053-2005, 2005.

ACPD
15, 10553–10592, 2015

Kirchstetter, T. W., Harley, R. A., Kreisberg, N. M., Stolzenburg, M. R., and Hering, S. V.: On-road measurement of fine particle and nitrogen oxide emissions from light- and heavy-duty motor vehicles, Atmos. Environ., 33, 2955–2968, doi:10.1016/S1352-2310(99)00089-8, 1999.

Kroll, J. H., Chan, A. W. H., Ng, N. L., Flagan, R. C., and Seinfeld, J. H.: Reactions of semivolatile organics and their effects on secondary organic aerosol formation, Environ. Sci. Technol., 41, 3545–3550, doi:10.1021/es062059x, 2007.

Kroll, J. H., Smith, J. D., Worsnop, D. R., and Wilson, K. R.: Characterisation of lightly oxidised organic aerosol formed from the photochemical aging of diesel exhaust particles, Environ. Chem., 9, 211–220, doi:10.1071/EN11162, 2012.

Lindinger, W., Hansel, A., and Jordan, A.: On-line monitoring of volatile organic compounds at pptv levels by means of proton-transfer-reaction mass spectrometry (PTR-MS) medical applications, food control and environmental research, Int. J. Mass Spectrom., 173, 191–241, doi:10.1016/S0168-1176(97)00281-4, 1998.

Lu, Z., Hao, J., Takekawa, H., Hu, L., and Li, J.: Effect of high concentrations of inorganic seed aerosols on secondary organic aerosol formation in the *m*-xylene/NO_x photooxidation system, Atmos. Environ., 43, 897–904, 2009.

McFiggans, G., Artaxo, P., Baltensperger, U., Coe, H., Facchini, M. C., Feingold, G., Fuzzi, S., Gysel, M., Laaksonen, A., Lohmann, U., Mentel, T. F., Murphy, D. M., O'Dowd, C. D., Snider, J. R., and Weingartner, E.: The effect of physical and chemical aerosol properties on warm cloud droplet activation, Atmos. Chem. Phys., 6, 2593–2649, doi:10.5194/acp-6-2593-2006, 2006.

McMurry, P. H. and Grosjean, D.: Gas and aerosol wall losses in Teflon film smog chambers, Environ. Sci. Technol., 19, 1176–1182, doi:10.1021/es00142a006, 1985.

Miracolo, M. A., Presto, A. A., Lambe, A. T., Hennigan, C. J., Donahue, N. M., Kroll, J. H., Worsnop, D. R., and Robinson, A. L.: Photo-oxidation of low-volatility organics found in motor vehicle emissions: production and chemical evolution of organic aerosol mass, Environ. Sci. Technol., 44, 1638–1643, doi:10.1021/es902635c, 2010.

Nakao, S., Shrivastava, M., Nguyen, A., Jung, H., and Cocker, D.: Interpretation of secondary organic aerosol formation from diesel exhaust photooxidation in an environmental chamber, Aerosol. Sci. Tech., 45, 964–972, doi:10.1080/02786826.2011.573510, 2011.

National Bureau of Statistics of China: China Statistical Yearbook, China Statistics Press, Beijing, 2013.

ACPD
15, 10553–10592, 2015

Ng, N. L., Kroll, J. H., Chan, A. W. H., Chhabra, P. S., Flagan, R. C., and Seinfeld, J. H.: Secondary organic aerosol formation from *m*-xylene, toluene, and benzene, Atmos. Chem. Phys., 7, 3909–3922, doi:10.5194/acp-7-3909-2007, 2007.

Ng, N. L., Canagaratna, M. R., Zhang, Q., Jimenez, J. L., Tian, J., Ulbrich, I. M., Kroll, J. H., Docherty, K. S., Chhabra, P. S., Bahreini, R., Murphy, S. M., Seinfeld, J. H., Hildebrandt, L., Donahue, N. M., DeCarlo, P. F., Lanz, V. A., Prévôt, A. S. H., Dinar, E., Rudich, Y., and Worsnop, D. R.: Organic aerosol components observed in Northern Hemispheric datasets from Aerosol Mass Spectrometry, Atmos. Chem. Phys., 10, 4625–4641, doi:10.5194/acp-10-4625-2010, 2010.

Ng, N. L., Canagaratna, M. R., Jimenez, J. L., Chhabra, P. S., Seinfeld, J. H., and Worsnop, D. R.: Changes in organic aerosol composition with aging inferred from aerosol mass spectra, Atmos. Chem. Phys., 11, 6465–6474, doi:10.5194/acp-11-6465-2011, 2011.

Nordin, E. Z., Eriksson, A. C., Roldin, P., Nilsson, P. T., Carlsson, J. E., Kajos, M. K., Hellén, H., Wittbom, C., Rissler, J., Löndahl, J., Swietlicki, E., Svenningsson, B., Bohgard, M., Kulmala, M., Hallquist, M., and Pagels, J. H.: Secondary organic aerosol formation from idling gasoline passenger vehicle emissions investigated in a smog chamber, Atmos. Chem. Phys., 13, 6101–6116, doi:10.5194/acp-13-6101-2013, 2013.

Odum, J. R., Hoffmann, T., Bowman, F., Collins, D., Flagan, R. C., and Seinfeld, J. H.: Gas/particle partitioning and secondary organic aerosol yields, Environ. Sci. Technol., 30, 2580–2585, doi:10.1021/es950943+, 1996.

Odum, J. R., Jungkamp, T. P. W., Griffin, R. J., Forstner, H. J. L., Flagan, R. C., and Seinfeld, J. H.: Aromatics, reformulated gasoline, and atmospheric organic aerosol formation, Environ. Sci. Technol., 31, 1890–1897, doi:10.1021/es960535l, 1997.

Pankow, J. F.: An absorption-model of gas-particle partitioning of organic compounds in the atmosphere, Atmos. Environ., 28, 185–188, 1994a.

Pankow, J. F.: An absorption-model of the gas aerosol partitioning involved in the formation of secondary organic aerosol, Atmos. Environ., 28, 189–193, 1994b.

Pathak, R. K., Stanier, C. O., Donahue, N. M., and Pandis, S. N.: Ozonolysis of α-pinene at atmospherically relevant concentrations: Temperature dependence of aerosol mass fractions (yields), J. Geophys. Res.-Atmos., 112, D03201, doi:10.1029/2006jd007436, 2007.

Platt, S. M., El Haddad, I., Zardini, A. A., Clairotte, M., Astorga, C., Wolf, R., Slowik, J. G., Temime-Roussel, B., Marchand, N., Ježek, I., Drinovec, L., Močnik, G., Möhler, O., Richter, R., Barmet, P., Bianchi, F., Baltensperger, U., and Prévôt, A. S. H.: Secondary or-

ACPD
15, 10553–10592, 2015

ganic aerosol formation from gasoline vehicle emissions in a new mobile environmental reaction chamber, Atmos. Chem. Phys., 13, 9141–9158, doi:10.5194/acp-13-9141-2013, 2013.
Presto, A. A., Gordon, T. D., and Robinson, A. L.: Primary to secondary organic aerosol: evolution of organic emissions from mobile combustion sources, Atmos. Chem. Phys., 14, 5015–5036, doi:10.5194/acp-14-5015-2014, 2014.
Robinson, A. L., Donahue, N. M., Shrivastava, M. K., Weitkamp, E. A., Sage, A. M., Grieshop, A. P., Lane, T. E., Pierce, J. R., and Pandis, S. N.: Rethinking organic aerosols: semivolatile emissions and photochemical aging, Science, 315, 1259–1262, doi:10.1126/science.1133061, 2007.
Samy, S. and Zielinska, B.: Secondary organic aerosol production from modern diesel engine emissions, Atmos. Chem. Phys., 10, 609–625, doi:10.5194/acp-10-609-2010, 2010.
Saxena, P. and Hildemann, L.: Water-soluble organics in atmospheric particles: a critical review of the literature and application of thermodynamics to identify candidate compounds, J. Atmos. Chem., 24, 57–109, doi:10.1007/BF00053823, 1996.
Schauer, J. J., Kleeman, M. J., Cass, G. R., and Simoneit, B. R. T.: Measurement of emissions from air pollution sources, 5. C1–C32 organic compounds from gasoline-powered motor vehicles, Environ. Sci. Technol., 36, 1169–1180, doi:10.1021/es0108077, 2002.
Shakya, K. M. and Griffin, R. J.: Secondary organic aerosol from photooxidation of polycyclic aromatic hydrocarbons, Environ. Sci. Technol., 44, 8134–8139, doi:10.1021/es1019417, 2010.
Song, C., Na, K., Warren, B., Malloy, Q., and Cocker, D. R.: Impact of propene on secondary organic aerosol formation from *m*-xylene, Environ. Sci. Technol., 41, 6990–6995, doi:10.1021/es062279a, 2007.
Tkacik, D. S., Presto, A. A., Donahue, N. M., and Robinson, A. L.: Secondary organic aerosol formation from intermediate-volatility organic compounds: cyclic, linear, and branched alkanes, Environ. Sci. Technol., 46, 8773–8781, doi:10.1021/es301112c, 2012.
Tkacik, D. S., Lambe, A. T., Jathar, S., Li, X., Presto, A. A., Zhao, Y. L., Blake, D., Meinardi, S., Jayne, J. T., Croteau, P. L., and Robinson, A. L.: Secondary Organic Aerosol Formation from in-Use Motor Vehicle Emissions Using a Potential Aerosol Mass Reactor, Environ. Sci. Technol., 48, 11235–11242, doi:10.1021/es502239v, 2014.
Tong, H. Y., Hung, W. T., and Cheung, C. S.: On-road motor vehicle emissions and fuel consumption in urban driving conditions, JAPCA J. Air Waste Ma., 50, 543–554, 2000.

ACPD
15, 10553–10592, 2015

Volkamer, R., Jimenez, J. L., San Martini, F., Dzepina, K., Zhang, Q., Salcedo, D., Molina, L. T., Worsnop, D. R., and Molina, M. J.: Secondary organic aerosol formation from anthropogenic air pollution: rapid and higher than expected, Geophys. Res. Lett., 33, L17811, doi:10.1029/2006gl026899, 2006.

Wang, X. M. and Wu. T.: Release of isoprene and monoterpenes during the aerobic decomposition of orange wastes from laboratory incubation experiments, Environ. Sci. Technol., 42, 3265–3270, 2008.

Wang, X. H., Bi, X. H., Sheng, G. Y., and Fu, J. M.: Chemical composition and sources of PM_{10} and $PM_{2.5}$ aerosols in Guangzhou, China, Environ. Monit. Assess., 119, 425–439, doi:10.1007/s10661-005-9034-3, 2006.

Wang, X., Liu, T., Bernard, F., Ding, X., Wen, S., Zhang, Y., Zhang, Z., He, Q., Lü, S., Chen, J., Saunders, S., and Yu, J.: Design and characterization of a smog chamber for studying gas-phase chemical mechanisms and aerosol formation, Atmos. Meas. Tech., 7, 301–313, doi:10.5194/amt-7-301-2014, 2014.

Weitkamp, E. A., Sage, A. M., Pierce, J. R., Donahue, N. M., and Robinson, A. L.: Organic aerosol formation from photochemical oxidation of diesel exhaust in a smog chamber, Environ. Sci. Technol., 41, 6969–6975, doi:10.1021/es070193r, 2007.

Yang, H., Yu, J. Z., Ho, S. S. H., Xu, J. H., Wu, W. S., Wan, C. H., Wang, X. D., Wang, X. R., and Wang, L. S.: The chemical composition of inorganic and carbonaceous materials in $PM_{2.5}$ in Nanjing, China, Atmos. Environ., 39, 3735–3749, doi:10.1016/j.atmosenv.2005.03.010, 2005.

Yi, Z., Wang, X., Sheng, G., Zhang, D., Zhou, G., and Fu, J.: Soil uptake of carbonyl sulfide in subtropical forests with different successional stages in south China, J. Geophys. Res., 112, D08302, doi:10.1029/2006JD008048, 2007.

Zhang, Q., Worsnop, D. R., Canagaratna, M. R., and Jimenez, J. L.: Hydrocarbon-like and oxygenated organic aerosols in Pittsburgh: insights into sources and processes of organic aerosols, Atmos. Chem. Phys., 5, 3289–3311, doi:10.5194/acp-5-3289-2005, 2005.

Zhang, Q., Jimenez, J. L., Canagaratna, M. R., Allan, J. D., Coe, H., Ulbrich, I., Alfarra, M. R., Takami, A., Middlebrook, A. M., Sun, Y. L., Dzepina, K., Dunlea, E., Docherty, K., DeCarlo, P. F., Salcedo, D., Onasch, T., Jayne, J. T., Miyoshi, T., Shimono, A., Hatakeyama, S., Takegawa, N., Kondo, Y., Schneider, J., Drewnick, F., Borrmann, S., Weimer, S., Demerjian, K., Williams, P., Bower, K., Bahreini, R., Cottrell, L., Griffin, R. J., Rautiainen, J., Sun, J. Y., Zhang, Y. M., and Worsnop, D. R.: Ubiquity and dominance of oxygenated species

ACPD
15, 10553–10592, 2015

in organic aerosols in anthropogenically-influenced Northern Hemisphere midlatitudes, Geophys. Res. Lett., 34, L13801, doi:10.1029/2007gl029979, 2007.
Zhang, Q., He, K., and Huo, H.: Policy: cleaning China's air, Nature, 484, 161–162, 2012.
Zhang, Y. L., Guo, H., Wang, X. M., Simpson, I. J., Barletta, B., Blake, D. R., Meinardi, S., Rowland, F. S., Cheng, H. R., Saunders, S. M., and Lam, S. H. M.: Emission patterns and spatiotemporal variations of halocarbons in the Pearl River Delta region, southern China, J. Geophys. Res., 115, D15309, doi:10.1029/2009JD013726, 2010.
Zhang, Y., Wang, X., Blake, D. R., Li, L., Zhang, Z., Wang, S., Guo, H., Lee, F. S. C., Gao, B., Chan, L., Wu, D., and Rowland, F. S.: Aromatic hydrocarbons as ozone precursors before and after outbreak of the 2008 financial crisis in the Pearl River Delta region, south China, J. Geophys. Res., 117, D15306, doi:10.1029/2011JD017356, 2012.
Zhang, Y., Wang, X., Zhang, Z., Lü, S., Shao, M., Lee, F. S. C., and Yu, J.: Species profiles and normalized reactivity of volatile organic compounds from gasoline evaporation in China, Atmos. Environ., 79, 110–118, doi:10.1016/j.atmosenv.2013.06.029, 2013.
Zhang, Y. L., Wang, X. M., Li, G. H., Yang, W. Q., Huang, Z. H., Zhang, Z., Huang, X. Y., Deng, W., Liu, T. Y., Huang, Z. Z., and Zhang, Z. Y.: Emission factors of fine particles, carbonaceous aerosols and traces gases from road vehicles: recent tests in an urban tunnel in the Pearl River Delta, China, Atmos. Environ., in review, 2015.

ACPD
15, 10553–10592, 2015

Table 1. Detailed information of the two light-duty gasoline vehicles.

ID	Emission standard class	Vehicle	Model year	Mileage (km)	Displacement (cm^3)	Power (kW)	Weight (kg)
I	Euro4	Golf	2011	25 000	1598	77	1295
II	Euro1	Accord	2002	237 984	2298	110	1423

ACPD
15, 10553–10592, 2015

Table 2. Initial conditions for the light-duty gasoline vehicle photooxidation experiments.

Experiment #	Vehicle ID	T (°C)	RH (%)	VOC/ NO_x	NMHCs (ppbv)	NO (ppbv)	NO_2 (ppbv)
1	I	25.8	52.0	10.2	1368	115.1	18.4
2	II	24.1	57.0	6.0	2583	431.0	0.6
3	I	25.0	52.9	9.3	2896	300.6	9.5
4	I	24.2	52.5	2.0	1885	794.1	161.9
5	II	25.0	52.6	7.2	1507	210.4	0.7

ACPD
15, 10553–10592, 2015

Table 3. The predicted SOA production from each aromatic hydrocarbon in all experiments.

		Experiment				
		1	2	3	4	5
	Species	Predicted SOA ($\mu g\,m^{-3}$)				
	benzene	1.6	0.1	1.5	1.9	0.0
	toluene	7.7	0.5	7.3	7.6	0.2
C2–benzene	ethyl-benzene	1.3	0.4	0.5	3.0	0.0
	m-, *p*-Xylene	2.9	1.7	2.8	7.6	0.2
	styrene	1.0	0.3	2.8	2.2	0.0
	o-Xylene	0.9	0.7	1.1	2.9	0.0
C3–benzene	isopropylbenzene	0.1	0.1	0.1	0.2	0.0
	n-propylbenzene	0.2	0.3	0.0	0.6	0.0
	m-ethyltoluene	1.4	1.6	3.1	7.4	0.2
	p-ethyltoluene	0.3	1.1	0.5	1.9	0.0
	1,3,5-trimethyl-benzene	0.8	1.2	3.4	3.0	0.1
	o-ethyltoluene	0.5	0.8	0.6	2.5	0.0
	1,2,4-trimethylbenzene	2.1	2.6	9.7	10.2	0.3
	1,2,3-trimethylbenzene	0.6	0.9	3.9	2.4	0.1
C4–benzene	m-diethylbenzene	0.1	0.4	0.2	0.2	0.0
	p-diethylbenzene	0.1	0.6	0.0	0.7	0.1
	o-diethylbenzene	0.0	0.0	0.0	0.1	0.0
	naphthalene	20.7	2.7	8.0	9.7	2.1
	total predicted SOA	42.2	15.9	45.5	63.9	3.4
	total measured SOA	51.1	17.6	77.6	125.4	4.0

ACPD
15, 10553–10592, 2015

Table 4. Summary of the results for the light-duty gasoline vehicle photooxidation experiments.

Exp #	Vehicle ID	OH ($\times 10^6$ molecules cm^{-3})	POA (μg m^{-3})	SOA (μg m^{-3})	SOA/POA	Effective yield
1	I	1.23	1.1	51.1	46	0.103
2	II	0.73	0.2	17.6	88	0.038
3	I	0.88	0.3	77.6	259	0.119
4	I	1.20	1.0	125.4	125	0.172
5	II	0.79	0.3	4.0	12	0.028

ACPD
15, 10553–10592, 2015

Table 5. Chemical compositions of the aromatic hydrocarbons in the exhaust of different vehicles, listed as weight percentages.

Species	I	II
Benzene	8.36	3.05
Toluene	8.38	3.88
C2–benzene	7.93	5.47
C3–benzene	10.00	8.66
C4–benzene	0.23	0.53
Naphthalene	3.06	0.95

ACPD
15, 10553–10592, 2015

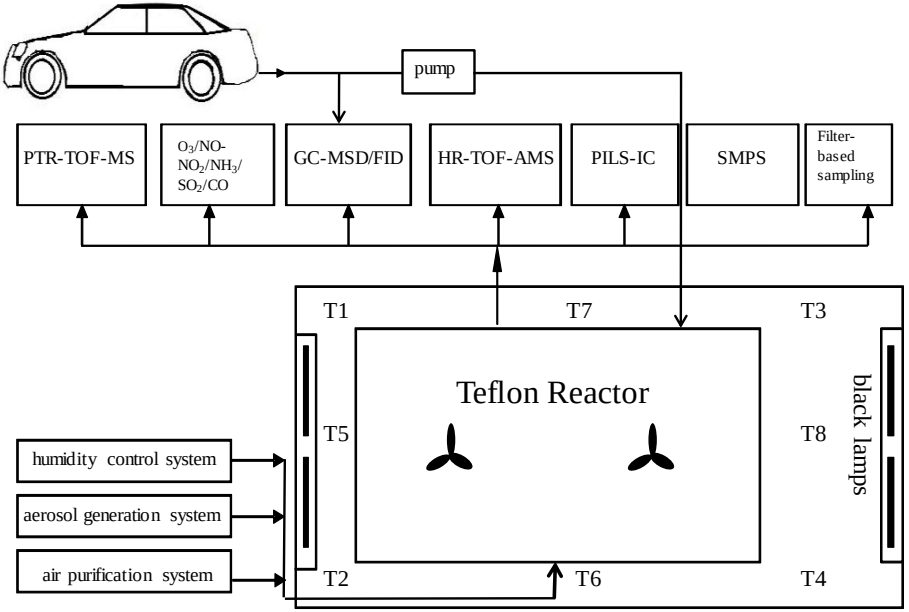

Figure 1. Schematic of the GIG-CAS smog chamber facility and vehicle exhaust injection system.

ACPD
15, 10553–10592, 2015

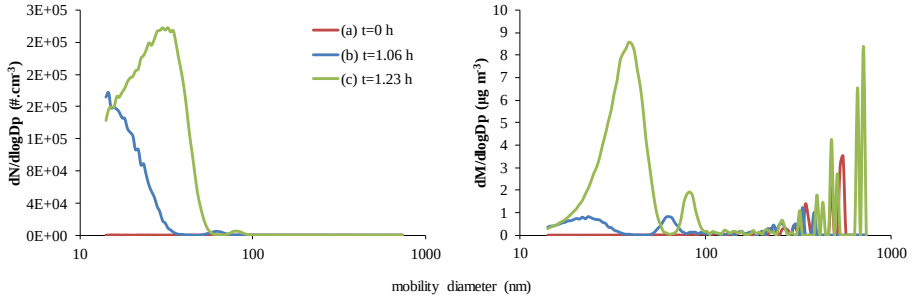

Figure 2. Particle number (left) and mass (right) distributions for a typical smog chamber experiment (experiment 2). **(a)** just before black lamps were turned on, **(b)** at the beginning of a nucleation event about 1 h after black lamps were turned on, **(c)** 10 min after the nucleation.

ACPD
15, 10553–10592, 2015

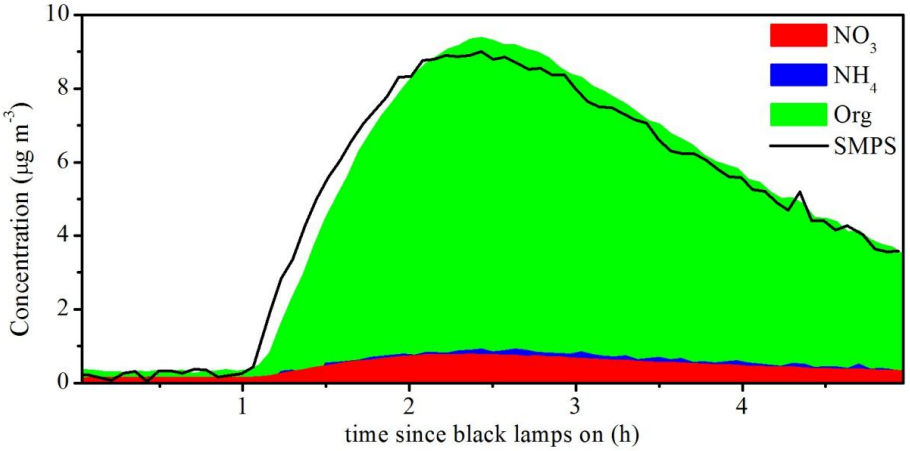

Figure 3. Comparison of the sum of organics, nitrate and ammonium (measured by AMS) against the total particle mass measured by the SMPS for experiment 2. Data are not wall-loss corrected.

ACPD
15, 10553–10592, 2015

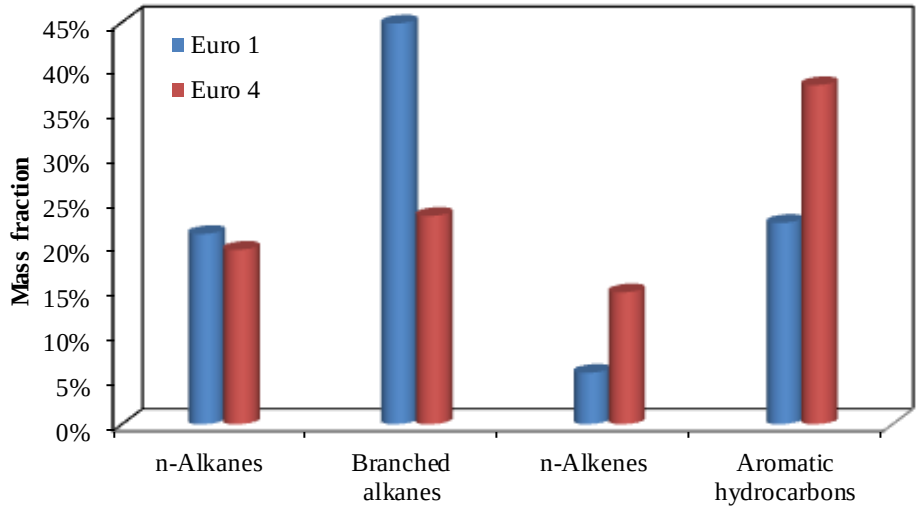

Figure 4. Composition of gasoline vehicle exhausts from Euro 1 and Euro 4 private cars.

ACPD
15, 10553–10592, 2015

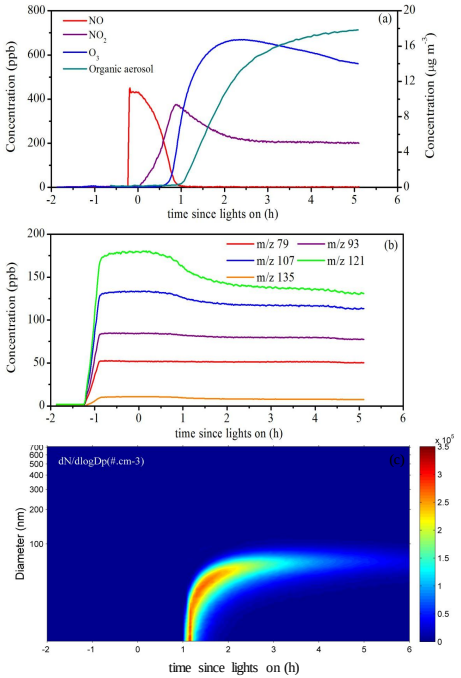

Figure 5. Concentration–time plots of gas–phase and particle–phase species and particle number concentration distribution as a function of time during a typical smog chamber experiment (experiment 2): **(a)** NO, NO_2, O_3 (left y axis) and organic aerosol (right y axis); **(b)** gas-phase light aromatics (benzene characterized by m/z 79; toluene characterized by m/z 93; C_2–benzene characterized by m/z 107; C_3–benzene characterized by m/z 121; C_4–benzene characterized by m/z 135); **(c)** particle size-number concentration distributions as a function of time. The vehicle exhaust was introduced into the reactor between −1.3 and −0.85 h; the primary emissions were characterized from −0.85 to 0 h; at time = 0 h, the black lamps were turned on.

ACPD
15, 10553–10592, 2015

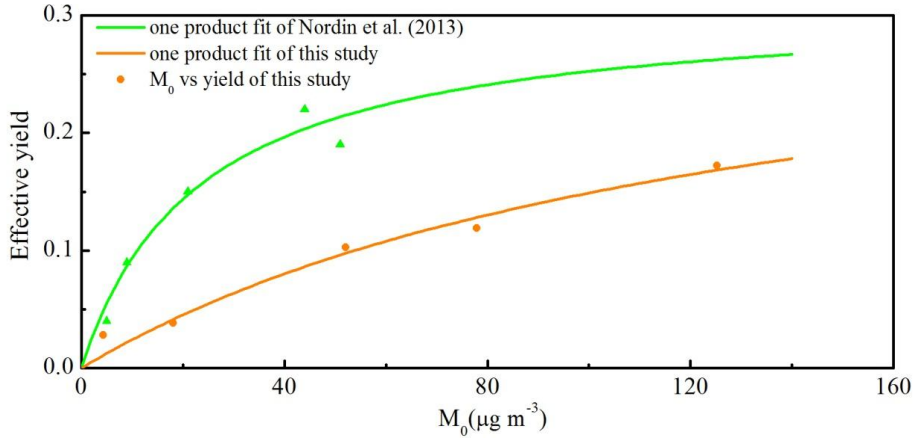

Figure 6. Comparison of yield data obtained for the gasoline experiments in this study with that of Nordin et al. (2013). The green line is the best fit one-product model (α_1 = 0.311, $K_{om,1}$ = 0.043) for the data set of Nordin et al. (2013). The orange line is the best one-product fit to the effective SOA yield in this study (α_1 = 0.350, $K_{om,1}$ = 0.007).

ACPD
15, 10553–10592, 2015

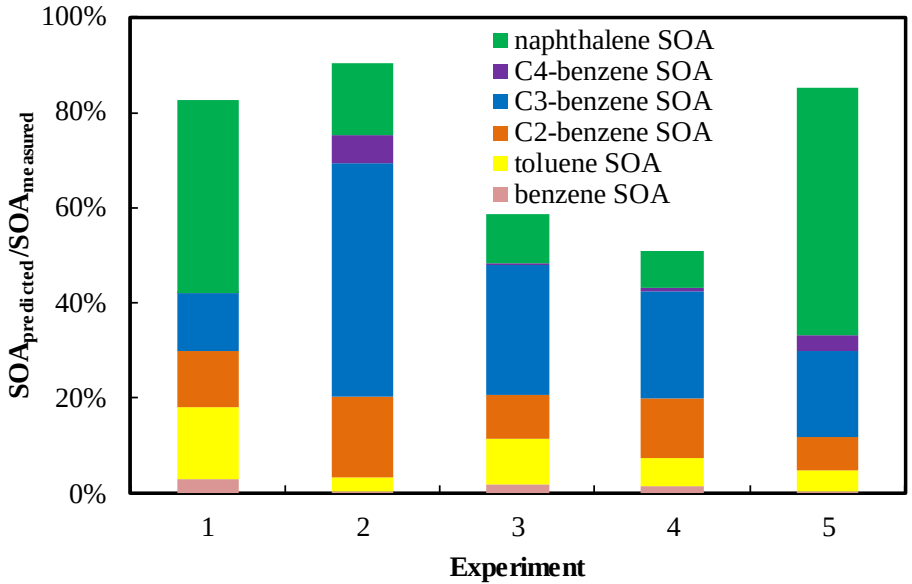

Figure 7. Contributions of the predicted benzene SOA, toluene SOA, C2–benzene SOA, C3–benzene SOA, C4–benzene SOA and naphthalene SOA to the total formed SOA in all experiments.

ACPD
15, 10553–10592, 2015

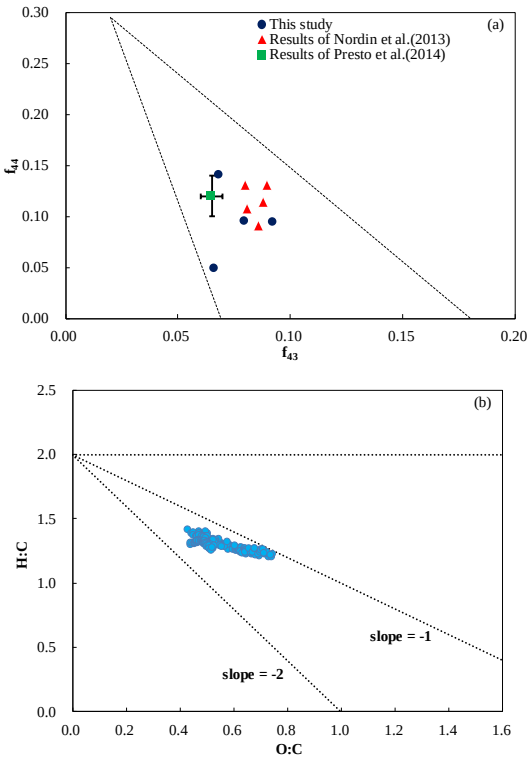

Figure 8. (a) The fractions of total organic signal at m/z 43 (f_{43}) vs. m/z (f_{44}) at the end of each experiment together with the triangle plot of Ng et al. (2010). The solid square and triangles represent the results of Presto et al. (2014) and Nordin et al. (2013), respectively. The dotted lines define the space where ambient OOA components fall. The ranges of f_{44} observed for SV-OOA and LV-OOA components are 0.03–0.11 and 0.13–0.21, respectively. **(b)** Van Krevelen diagram of SOA from light-duty gasoline vehicle exhaust. Dotted lines are to show slopes of 0, −1 and −2. AMS data of the experiment 5 were unavailable.

ACPD
15, 10553–10592, 2015